*Journal of Advanced Ceramics*
2019, **8**(1): 62–71
https://doi.org/10.1007/s40145-018-0291-3
ISSN 2226-4108
CN 10-1154/TQ

**Research Article**

# Step distribution of Yb filling fraction during microstructural evolution in skutterudites

Jing MEI[a], Zheng YAO[b], Shuya ZHU[a], Dongli HU[a], Ying JIANG[a], Juanjuan XING[a,*], Hui GU[a], Lidong CHEN[b]

[a]*School of Materials Science and Engineering and Materials Genome Institute, Shanghai University, Shanghai 200444, China*
[b]*State Key Laboratory of High Performance Ceramics and Superfine Microstructure, Shanghai Institute of Ceramics, Chinese Academy of Sciences, Shanghai 200050, China*

Received: March 5, 2018; Revised: June 21, 2018; Accepted: July 23, 2018


**Abstract:** To achieve a better material for thermoelectric power generation device, filled skutterudite $Yb_{0.3}Co_4Sb_{12}$ samples were fabricated by melting–quenching–annealing–spark plasma sintering (SPS) method. Two sets of samples, before and after SPS, were investigated. In both the two sets of samples, the average grain size of the samples increases monotonously with the increase of annealing time, while Yb filling fraction firstly increases and then decreases. Yb not filling into the skutterudite remains at the grain boundaries in the form of $Yb_2O_3$ after SPS, which could be quantified by the spatially difference method of energy dispersive spectra. Step distribution of Yb filling fraction was observed in the samples annealed for 1 h, which was caused by the microstructural evolution from the peritectic phases to the skutterudite phase. The sample annealed for 3 days and SPS sintered possesses the maximum value of Yb filling fraction 0.249 and the maximum ZT value of 1.24 at 850 K. These results are helpful to better understand the microstructural evolution and Yb filling behavior in skutterudite materials.

**Keywords:** skutterudite; ytterbium filling fraction; microstructure; step distribution

## 1 Introduction

With the introduction of the phonon glass electron crystal (PEGC) conception, filled skutterudites have been reported as promising thermoelectric materials due to their low lattice thermal conductivity and excellent electronic properties [1–6]. The fillers located at the voids of skutterudite lattice are loosely bonded with the host atoms and the rattling effect of filler atoms can scatter the heat-carrying phonon [7–9]. According to the difference in vibration frequency of different group filling atoms, the atoms can be divided into three types: alkali metal (Na [10], K [11], etc.), alkaline earth metal (Sr [12], Ba [13,14], etc.), rare earth metal (La [15–17], Ce [15,18], Eu [19,20], Sm [21,22], didymium [23], Pr [24], etc.). The vibrational frequencies of the same group atoms are close to each other，while the atoms in the different groups have different vibrational frequencies. Alkali metals are relatively high, followed by alkaline earth metals; rare earth metals are the lowest. The Yb atom is particularly unique because of the lowest vibration

* Corresponding author.
E-mail: xingjuanjuan@shu.edu.cn

frequency, which can be classified as the fourth category. The unique low vibration frequency makes it effectively scatter lattice phonons, which other atoms cannot match [25]. Therefore, $Yb_xCo_4Sb_{12}$ is considered as one of the best n-type single filled skutterudites with unique characteristics.

Although the Yb filled skutterudites have been extensively studied for a long time, the Yb filling fraction limit (FFL) is still controversial. The calculated filling fraction limit for Yb element in $CoSb_3$ is about 0.3 [26] using *ab initio* density functional calculations. Currently, the Yb FFL has been reported to range from 0.2 to 0.7 [27–34]. Indeed, rare earth filling fraction is strictly bound to electronic and thermodynamic issues, and it is generally recognized as strongly dependent on the oxidation number rather than on the ion chemical identity [35]. Despite the great efforts that have been devoted to improving the FFL and thermoelectric properties, attentions are also needed for the actual amount of fillers going into the voids. Beyond that, the research on the relevance of Yb filling fraction to microstructure evolution is not detailed and systematic enough. On the other hand, as far as the fabrication approach for filled skutterudites is concerned, the melting–quenching–annealing–spark plasma sintering (SPS) method is the most widely adopted and utilized. The ideal melting–quenching–annealing–SPS method requires that all elements are homogeneously distributed to provide the minimized diffusion paths to realize a sufficient and complete solid-state reaction during the annealing process. However, local inhomogeneity usually exists in skutterudite, which is strongly affected by preparation technique, such as thermal treatments [36]. Therefore, a systematic study on the microstructural evolution in the whole fabrication process would help us better understand the filling behavior of Yb and its relationship with the thermoelectric property. The previous work of Yao *et al.* [37] focused on the genomic effects of the quenching process on the microstructure and thermoelectric properties of $Yb_{0.3}Co_4Sb_{12}$ and found Co–Sb peritectic segregation in the quenching process contributes to the formation of second phases ($YbSb_2$/CoSb/$CoSb_2$/Sb) and to the poor thermoelectric performance in the final large-scale $Yb_{0.3}Co_4Sb_{12}$ products.

In this work, we aimed at the effects of annealing time and SPS on the microstructure and thermoelectric properties of $Yb_{0.3}Co_4Sb_{12}$. Step distribution of Yb filling fraction was observed in the sample annealed for a short time, which indicates the local inhomogeneous distribution of Yb. With the increase of the annealing time, the step distribution of Yb filling fraction changed to the normal distribution. Yb not filling into the skutterudite remained at the grain boundaries in the form of $Yb_2O_3$, which could be quantified by the spatial difference method of energy dispersive spectra (EDS). Moderate annealing time, which was 3 days in our case, can lead to the relatively small grain size and high Yb filling fraction, which are beneficial to the thermoelectric property of the sample with the ZT value 1.24 at 850 K. The results could help us to better understand the process of microstructural evolution.

## 2 Experimental

The Yb-filled skutterudite samples were prepared by melting–quenching–annealing–SPS method with the raw materials Yb (99.98%, ingot), Co (99.95%, shot), and Sb (99.99%, shot). The raw materials were weighed with the nominal composition $Yb_{0.3}Co_4Sb_{12}$ and loaded into quartz tube with carbon crucibles (inner diameter 15 mm). The tubes were sealed under a pressure of $10^{-3}$ Pa, heated to 1353 K, held at this temperature for 2 days, and quenched in a supersaturated salt ice–water solution. The quenched ingots were annealed at 973 K for different time (1 h, 1 day, 3 days, and 7 days), crushed and ground into powders, and then were finally consolidated by SPS at 883 K under a pressure of 60 MPa for 5 min. The samples after melting–quenching–annealing–SPS process were recorded as A0S, A1S, A3S, and A7S, respectively. The samples obtained just after melting–quenching–annealing process were named after A0, A1, A3, A7 for comparison, respectively.

X-ray diffraction (XRD) data were collected using X-ray diffractometer (Bruker D2 PHASER) with Cu Kα radiation in the range $10° \leqslant 2\theta \leqslant 80°$. The microstructures of samples were observed by the scanning electron microscope (Model Supra55, G300, Carl Zeiss, Germany). Composition analysis was characterized by energy dispersive spectrometer (EDS; Oxford, UK). The statistics of grain size were performed by the image analysis software (Image Pro Plus v6.0). The ZT values were calculated by the formula $ZT = \frac{S^2\sigma T}{\kappa}$, where $S$, $\sigma$, $\kappa$, and $T$ are the Seebeck coefficient, electrical conductivity, total thermal

conductivity, and absolute temperature, respectively. The electrical conductivity and Seebeck coefficient were measured using the standard 4-probe method (ULVAC ZEM-3) in He atmosphere. The thermal conductivity was calculated from the thermal diffusivity $D$, specific heat $C_p$, and density density $\rho$ according to the relationship $\kappa = DC_P\rho$. The densities of samples were measured using the Archimedean method. The thermal diffusivity $D$ and specific heat $C_p$ were measured with a laser flash method (Netzsch LFA 427) and differential scanning calorimetry (Shimadzu DSC-50), respectively. All the measurements were performed in a temperature range from room temperature to 850 K.

## 3 Results and discussion

### 3. 1 Microstructures

Figure 1 shows the XRD patterns of the samples A0S, A1S, A3S, and A7S, which experienced the melting–quenching–annealing–SPS fabrication process. All the diffraction peaks can be indexed to the $CoSb_3$ skutterudite phase. No significant peak of second phase appears.

Figures 2(a)–2(d) illustrate the backscattered electron (BSE) images of the samples A0S, A1S, A3S, A7S, respectively. It is clearly seen that there are also some white areas besides the matrix grains in all the samples. The white areas were determined to be the second phase $Yb_2O_3$ by EDS. Such an inconsistency in XRD and SEM results might be due to the low volume content of second phase in the skutterudite composites, which is beyond the measurement limit of our XRD system. It is obvious that the $Yb_2O_3$ volume fraction shows a decreasing trend. In the sample A0S, $Yb_2O_3$ presents massive and continuous distribution in some regions (Fig. 2(a)), while $Yb_2O_3$ distributes sporadically in the samples A3S and A7S. The variation of $Yb_2O_3$ distribution indicates that the filling of Yb into the skutterudite becomes more and more homogeneous. The contrast of skutterudite grains is different as shown in Fig. 2, which might be caused by the difference of grain orientation. From the BSE images, it is obvious that the grain size increases with the increase of annealing time. Figure 3 gives the grain size distributions of the samples in detail. In contrast to the sample A0S, the grain size of the samples A1S, A3S, and A7S is relatively widely distributed. The sample A0S has a minimum average grain size of 2.12 μm and the sample A7S has a maximum average grain size of 4.87 μm. The data of the average grain sizes can be seen in Table 1.

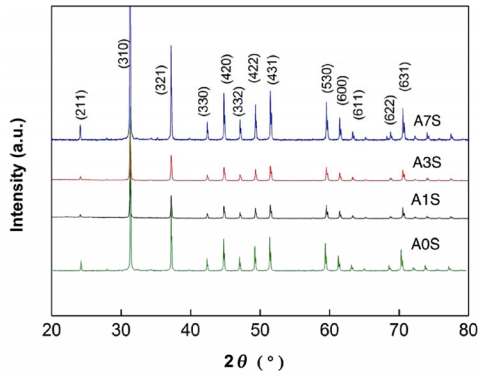


**Fig. 1** XRD patterns of the samples A0S, A1S, A3S, and A7S.

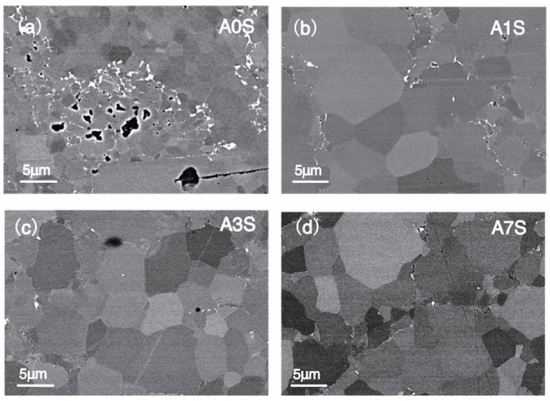


**Fig. 2** BSE images of the samples A0S, A1S, A3S, and A7S.

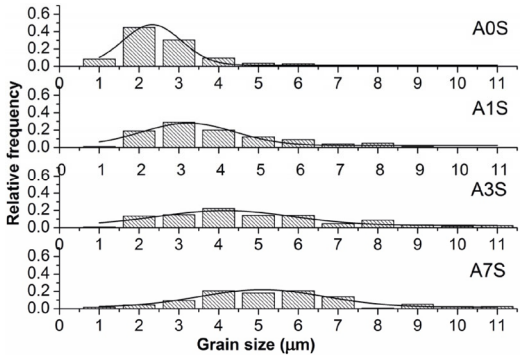


**Fig. 3** Grain size distributions of the samples A0S, A1S, A3S, and A7S.

**Table 1 Average grain size and Yb filling fraction of the samples**

| Annealing time | | 1 h | 1 day | 3 days | 7 days |
|---|---|---|---|---|---|
| Grain size (μm) | A | 1.50±0.67* | 4.23±2.13 | 4.60±2.27 | 5.03±2.37 |
| | AS | 2.12±1.07 | 3.46±1.77 | 4.36±2.25 | 4.87±2.10 |
| Yb filling fraction | A | 0.189±0.074* | 0.206±0.029 | 0.221±0.029 | 0.215±0.050 |
| | AS | 0.190±0.020 | 0.218±0.028 | 0.249±0.022 | 0.235±0.019 |

*The data just measured from the areas of skutterudite phase.

### 3. 2 Yb filling fraction

To investigate the exact filling of Yb, EDS analyses were performed in the $Yb_{0.3}Co_4Sb_{12}$ samples. In every sample, about 100 grains were detected. At least three points were measured in one grain, and the average value was taken as the Yb filling fraction in the grain. The detected Yb filling fractions of the $Yb_{0.3}Co_4Sb_{12}$ sample after annealing with different time and the same SPS process are shown in Fig. 4. The Yb filling fraction shows the normal distribution in the sample A0S (Fig. 4(a)) in contrast to the clear step distribution in the sample A1S. The frequencies of relatively lower Yb filling fraction are much lower in the sample A1S, while the frequencies of Yb filling fraction ranging from 0.175 to 0.25 are high and remain relatively flat. In the sample A3S, the Yb filling fraction presents Gaussian-like distribution and centralizes in 0.25 approximately. In the sample A7S, the frequency of Yb filling fraction over 0.275 is quite low. The average Yb filling fractions in every sample are summarized in Table 1. With the increase of annealing time, Yb filling fraction increases firstly, reaches the maximum (0.249) in the sample A3S, and then decreases a little in the sample A7S. The lowest Yb filling fraction in A0S indicates that the annealing time 1 h is not enough for Yb to enter the void of octahedral, which is consistent with the existence of amounts of $Yb_2O_3$ as shown in Fig. 2(a).

Obviously, Yb filling fractions in all the samples are lower than the nominal value. Except filling the skutterudite and forming the second phase $Yb_2O_3$, Yb was also found at the grain boundaries. Figure 5 reflects the change of Yb at the grain boundaries in the sample A0S. As shown in Figs. 5(b) and 5(c), the Yb content does not change across the grain boundary without white contrast (line 1 in Fig. 5(a)). In contrast, Yb strongly segregates to the grain boundary with white contrast (line 2 in Fig. 5(a)), which is clearly displayed in Figs. 5(d) and 5(e). Similar cases were also observed in the samples A1S, A3S, and A7S. Yb segregation to grain boundaries can be quantified by the method described in Refs. [38,39] by the formula:

$$\Gamma_i = \frac{K_i}{K_r}\left(\frac{I_i^{\text{on}}}{I_r^{\text{on}}} - \frac{I_i^{\text{off}}}{I_r^{\text{off}}}\right) \times \frac{M_r}{M_i} \times N_r^b \times w \qquad (1)$$

where $\Gamma_i$ is the excess level of element *i* segregated to the grain boundary. $K_i$ is the $\kappa$-factor of element *i*, $K_r$ is the $\kappa$-factor of the reference element *r* (the latter is Co in this study). $I_i$ and $I_r$ are the measured intensities of the corresponding elements; the superscripts on and off denote the positions of grain boundary and the two neighboring grains from where the data were collected, respectively. $M_i$ and $M_r$ are the atomic weights of respective elements. $N_r^b$ is the site

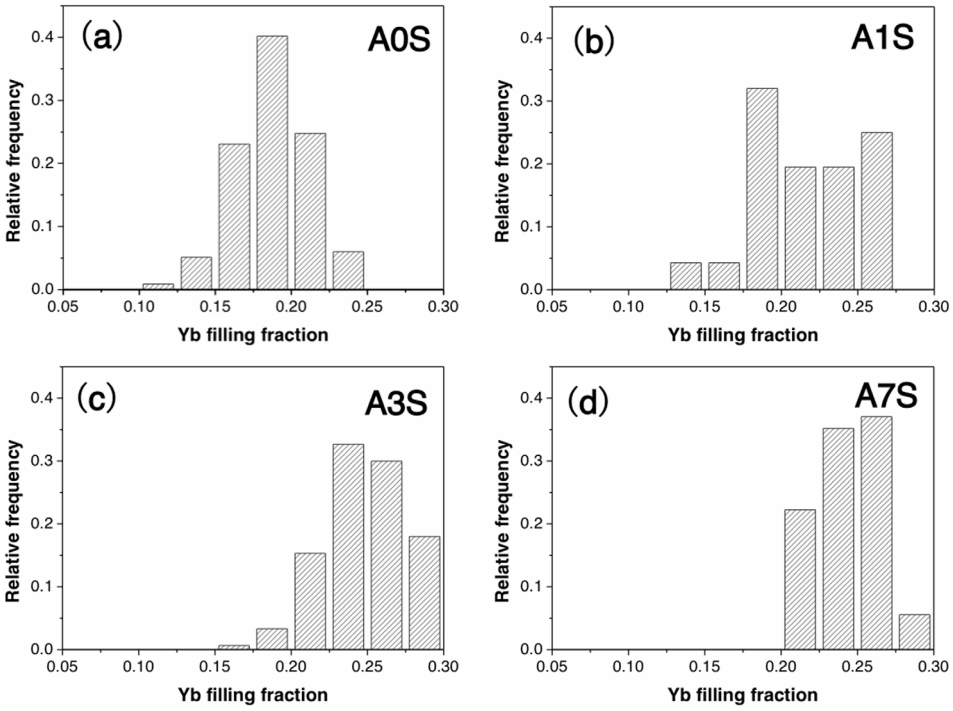


**Fig. 4** Yb filling fraction distribution in the samples A0S, A1S, A3S, and A7S.

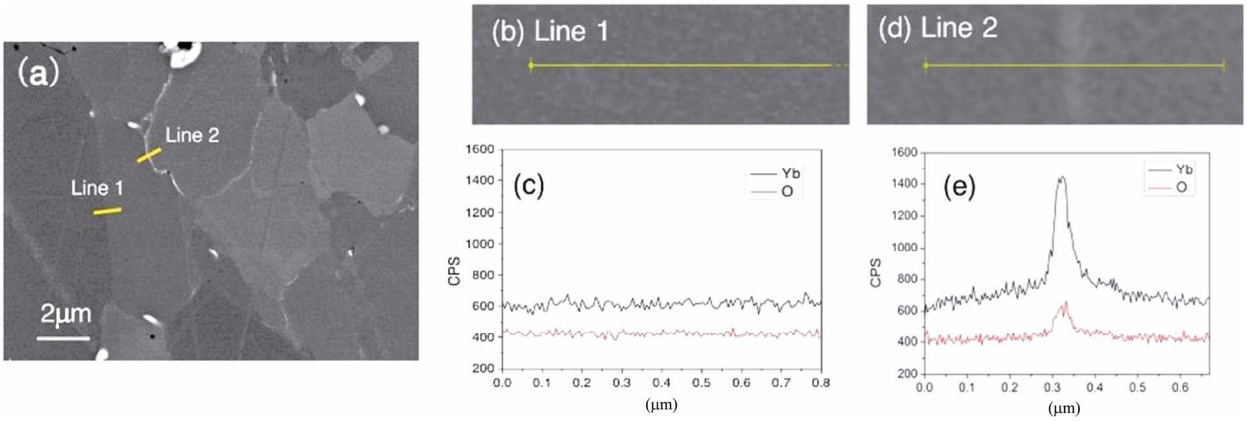


**Fig. 5** (a) A BSE image collected in the sample A0S; (b) the partial enlarged image of line 1; (c) scanning data of Yb and O in line 1; (d) the partial enlarged image of line 2; (e) scanning data of Yb and O in line 2.

density of the reference element Co, which is 5.412 $nm^{-3}$ in the $Co_4Sb_{12}$ phase, and $w$ is the width of rectangle used for the detection.

Taking the grain boundary shown in Fig. 5(d) as example, Yb excess at the grain boundary was calculated to be 1147.8 $nm^{-2}$. If segregated Yb is supposed to exist in the form of $Yb_2O_3$, the chemical width of $Yb_2O_3$ can be calculated to be 102.48 nm by the fomula:

$$d = \frac{\Gamma_i}{N_{\mathrm{Yb}}} \tag{2}$$

where $N_{\mathrm{Yb}}$ is the site density of element Yb in the $Yb_2O_3$, which is 11.2 $nm^{-3}$. Such a value is consistent with the width observed by the microstructural image shown in Fig. 5(d).

### 3. 3 Microstructural evolution

To make clear of the microstructural evolution process, especially Yb filling fraction, the analyses of the samples (A0, A1, A3, and A7) before the SPS process were conducted as follows to make comparison. Figure 6 shows the BSE images of the samples A0, A1, A3, and A7, which just experienced melting–quenching–annealing process. Compared to the samples after SPS, there are more pores in these samples. The densities are accordingly worse. It is notable that most regions in the sample A0 possess such a kind of morphology with equiaxed $CoSb_3$ grains as shown in Fig. 6(a). Besides that, there are still some regions in the sample A0 showing the peritectic characteristics [40] as presented in Fig. 7(a). The dark gray area is CoSb, which is wrapped in $CoSb_2$ (gray), and the large area of light gray is the Yb filled skutterudite phase. EDS mappings in Figs. 7(b), 7(c), and 7(d) clearly display the distribution of elements Yb, Sb, and Co in the three different phases. Such peritectic microstructure indicates that annealing 1 h is not sufficient for the solid state

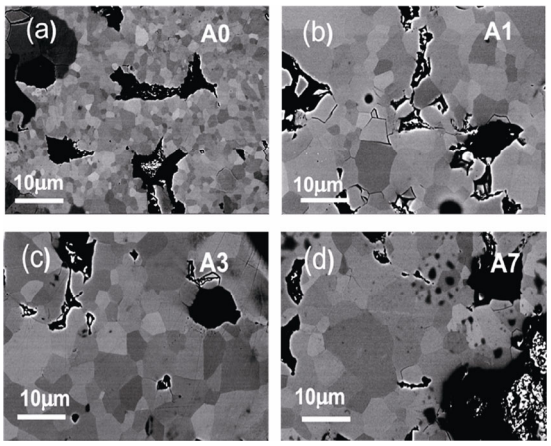


**Fig. 6** BSE images of the samples A0, A1, A3, and A7.

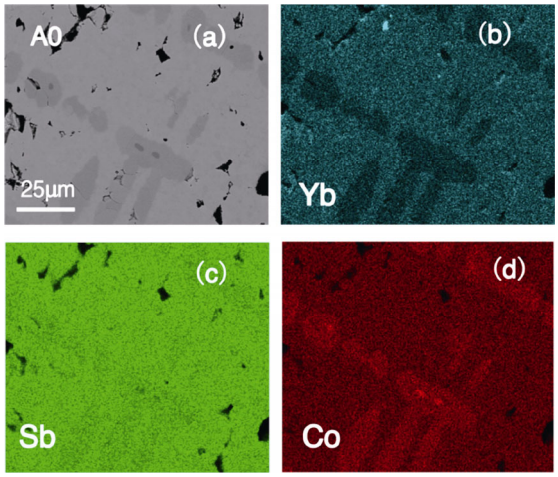


**Fig. 7** (a) A BSE image collected in the sample A0; (b), (c), and (d) EDS mappings of Yb, Sb, and Co elements, respectively.

reaction. In contrast, the A1, A3, and A7 samples get a relatively uniform skutterudite phase as displayed in Figs. 7(b), 7(c), and 7(d). Comparing the sample A0 with the sample A0S, it is found that peritectic characteristics (CoSb, $CoSb_2$) disappeared after SPS process. We speculate that the small amount of CoSb and $CoSb_2$ phases formed the non-stoichiometric $CoSb_{3-x}$ phase during the SPS process.

The average grain sizes of the samples before and after SPS are summarized in Table 1. It is noted that the grain size as well as Yb filling fraction of A0 sample were selective statistics, which were subsequently measured in the areas of skutterudite phase excluding the areas with peritectic microstructure. The common point between the two sets of samples lies in that the average grain size increases with the annealing time. Similar with the sample A0S, the sample A0 possesses the finest grains among the samples A0, A1, A3, and A7. For the sample A0, the remained peritectic microstructure and the smallest average grain size of selective skutterudite phase indicate that 1 h was too short for skutterudite phase formation and grain growth and A0 was far from the state of equilibrium. The following SPS process might enhance the grain growth a little bit: for the samples A1, A3, and A7, the skutterudite phase was completely formed and much closer to an equilibrium state compared with A0. The decrease of grain size after SPS process may be ascribed to the grinding process before SPS.

Not only the average grain size but also the Yb filling fractions in the samples before and after SPS are listed in Table 1. The Yb filling fraction firstly increases and then slightly decreases with the annealing time in both sets of samples. The maximums of Yb filling fraction in the two sets of samples are both reached when the annealing time is 3 days. The Yb filling fraction in the sample A0 is 0.189, much less than 0.221 in the sample A3, which indicates that the annealing time of 1 h is not enough for the reaction among the elements to form the final filled skutterudite phase. Therefore, the second phases CoSb and $CoSb_2$ remain in the sample A0 as shown in Fig. 7(a). The average Yb filling fraction in the sample A0S is 0.190, which is very close to that in the sample A0, but more homogeneous. Considering that there is no more second phase in the sample A0S, it is indicated that SPS process can promote the solid state reactions to form the Yb-filled $CoSb_3$. For the samples annealed for 1 day, 3 days, and 7 days, the Yb filling fractions are enhanced more or less by SPS process. The larger standard deviations of Yb filling fraction in the annealed samples (specially in A0 and A7) compared to SPS sintered samples indicates that the local composition is strongly affected by thermal treatments [36].

With the increase of annealing time, the cumulative curves of Yb filling fraction for the samples A0S, A1S, A3S, and A7S are presented in Fig. 8. Intuitively, it is interestingly found that the cumulative curve of the sample A1S presents step distribution. Yb filling fraction in the sample A1S distributes more widely than that in the samples A3S and A7S. Such step distribution might have a relationship with the accumulative influence of annealing and SPS process. As described above, there are two distinct microstructural characteristics in the sample A0 (Figs. 6(a) and 7(a)), and the distribution of Yb is therefore locally inhomogeneous in the different regions. Although Yb filling fraction presents a Gaussian-like distribution in the skutterudite phase areas in the sample A0 (Fig. 9(a)), the Yb filling fraction distribution changed a little in the sample A0S after SPS (Fig. 4(a)) indicating SPS promoted the formation $CoSb_{3-x}$ phase in the peritectic regions and homogenized the Yb filling fraction. When the annealing time was prolonged to 1 day, the peritectic regions as shown in the sample A0 might just disappeared, CoSb and $CoSb_2$ formed the non-stoichiometric $CoSb_{3-x}$ phase, and Yb at the grain boundaries (see next section) started to fill the newly formed skutterudite phase. On the other hand, Yb filling fraction in the previously formed skutterduite phase will be enhanced. Therefore, Yb filling fraction presents step distribution as shown in Fig. 9(b). Low Yb filling fraction with low relative frequency corresponds to the newly formed skutterudite phase. SPS process promoted the homogenization of relative high Yb filling fraction, but did not change the step distribution

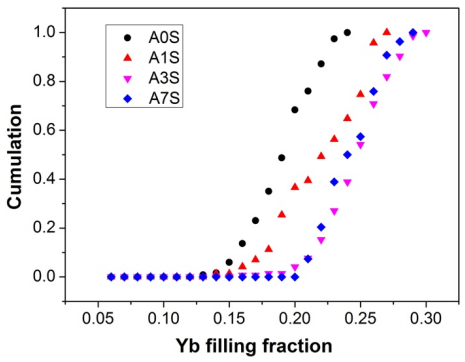


**Fig. 8** Accumulation curves of Yb filling fraction for the samples A0S, A1S, A3S, and A7S.

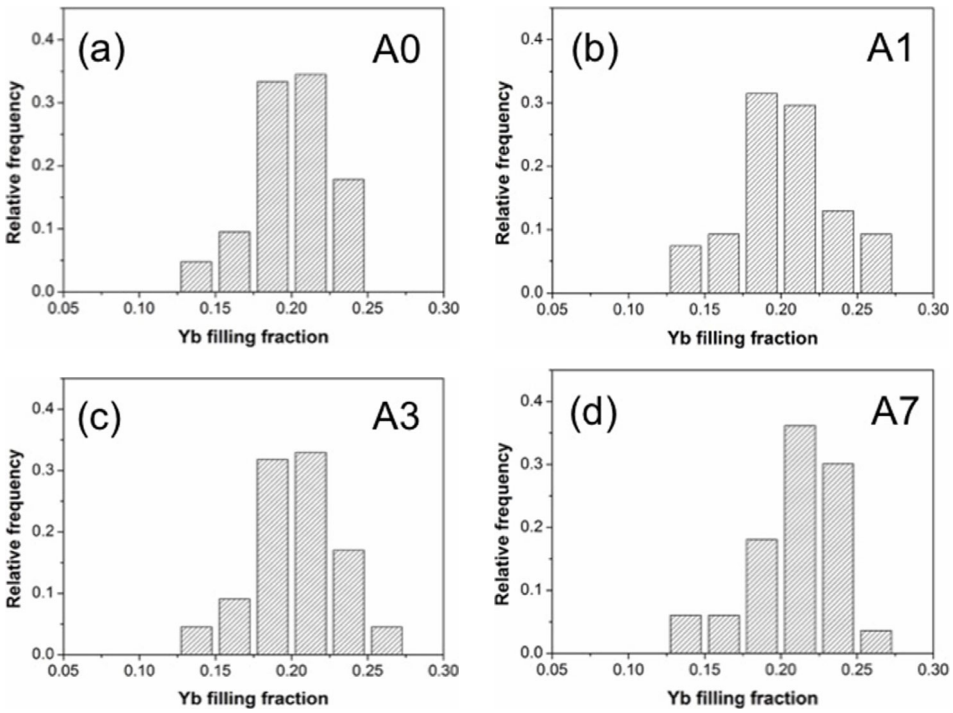


**Fig. 9** Yb filling fraction distribution in the samples A0, A1, A3, and A7. Note that the data of (a) just measured from the areas of skutterudite phase in the sample A0.

of Yb filling fraction (Fig. 4(b)). For the samples annealed for 3 and 7 days, the relatively uniform microstructure and homogenous Yb filling fraction could be obtained during the annealing process (Figs. 9(c) and 9(d)). After SPS, the microstructures changed little, and Yb filling fractions increased a bit (Figs. 4(c) and 4(d)).

### 3. 4 $Yb_2O_3$ formation

After SPS, $Yb_2O_3$ was formed in the samples A0S, A1S, A3S, and A7S. And the volume fraction of $Yb_2O_3$ in the microstructures shows a decreasing trend. Since the Yb filling fractions are all lower than the nominal value and there is no Yb-rich second phase in the samples A0, A1, A3, and A7, the rest of Yb is supposed to segregate to the grain boundaries. The lower Yb filling fraction in the grains indicates that the higher amounts of Yb distribute at the grain boundaries. During the process of crushing and grinding, intergranular fracture was easy to happen [41]. Yb at the grain boundaries would expose to the air and be oxidized. During SPS, $Yb_2O_3$ formed and aggregated at the boundaries or triple pockets. Since the Yb filling fraction in the sample A0 is the lowest, the $Yb_2O_3$ volume fraction in the sample A0S is the highest, as shown in Fig. 2. Inhomogeneous distribution of $Yb_2O_3$ in the microstructure originates from the inhomogeneous distribution of Yb at the grain boundaries before SPS.

### 3. 5 Thermoelectric properties

In addition, through these synergetic effects, the performance of the samples would be influenced. The temperature-dependent electrical conductivity, thermal conductivity, Seebeck coefficient, and ZT value are shown in Fig. 10. In order to ensure the accuracy of measurement, three samples were prepared for each set of test parameters and the mean and standard deviations were taken as the data points and error bars. From Fig. 10, we made the following observations: (I) the electrical conductivity of each sample decreases with temperature over the measured temperature range, indicating semi-metal or heavily doped features; (II) the thermal conductivity first decreases and then increases with temperature; (III) the absolute value of Seebeck coefficient increases with temperature and the negative Seebeck coefficient shows that electrons are the dominant charge carriers. The sample A0S has the lowest electrical conductivity and highest thermal conductivity, while the sample A3S has the highest electrical conductivity and lowest thermal conductivity. Comparing with the sample A7S, the sample A1S has higher electrical conductivity, which might be due to the step

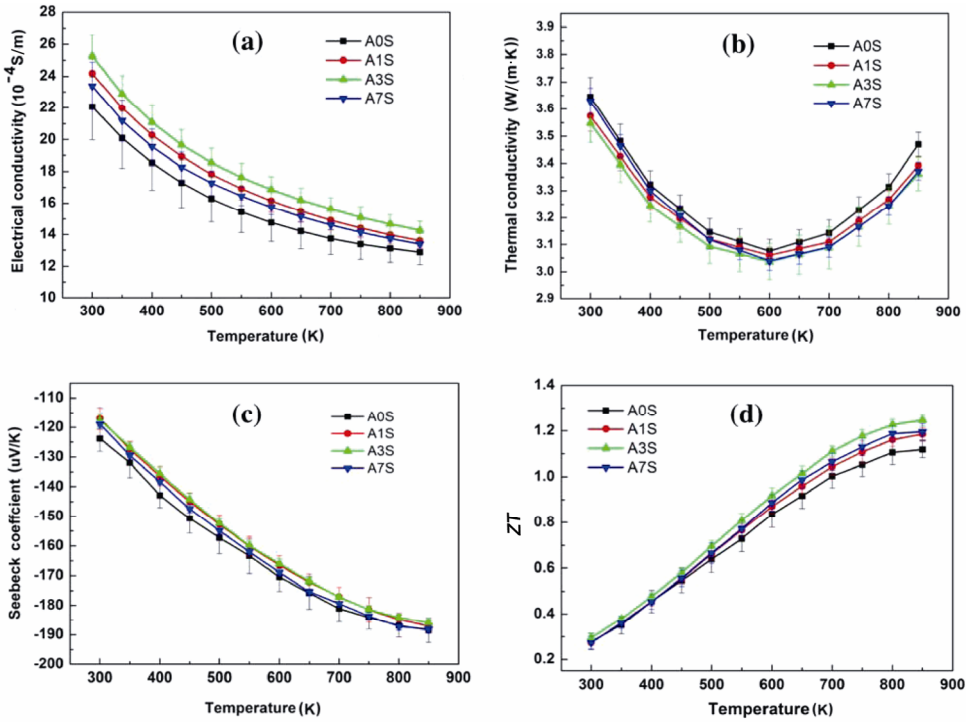


**Fig. 10** (a) Electrical conductivity, (b) thermal conductivity, (c) Seebeck coefficient, and (d) ZT value of the samples A0S, A1S, A3S, and A7S.

distribution of Yb filling fraction in the sample A1S. Although the sample A1S has the higher electrical conductivity, the lower thermal conductivity and the higher absolute value of Seebeck coefficient of the sample A7S lead to the higher ZT value over 550 ℃ (Fig. 10(d)). The value of ZT for each sample monotonously increases with temperature, reaches maximum around 850 K. For the samples A1S and A7S, the ZT values at 850 K are about 1.18, lower than the maximum value 1.24 of the sample A3S. From Fig. 10(d), it can be concluded that the ZT value is consistent with the Yb filling fraction. In the filled skutterudite samples, measured grain sizes of the samples are at the micrometer scale in Table 1, indicating that would not affect scatter process for electrons whose mean free path (approximately several nanometers) are much lower than the grain size [42]. The filling element Yb as an electron donor and phonon scatter center can effectively improve the electrical conductivity and reduce lattice thermal conductivity.

## 4 Conclusions

By melting–quenching–annealing–SPS method, filled-skutterudite $Yb_{0.3}Co_4Sb_{12}$ was prepared. Two sets of samples, before and after SPS, were investigated. In both sets of samples, the average grain size increases monotonously with the annealing time, while the filling fraction of Yb firstly increases and then decreases. Yb not filling into the skutterudite remained at the grain boundaries in the form of $Yb_2O_3$, which could be quantified by the spatially difference method of EDS. Step distribution of Yb filling fraction was observed in the sample annealed for 1 h, which was caused by the microstructural evolution from the peritectic phases into the skutterudite phase. The sample annealed for 3 days and SPS sintered possesses the maximum Yb filling fraction 0.249 and the maximum ZT value of 1.24 at 850 K.

## Acknowledgements

This work was financially supported by the National Natural Science Foundation of China under Grant Nos. 51532006 and 11704238, Shanghai Municipal Science and Technology Commission of Shanghai Municipality under Grant No. 16DZ2260601, and State Administration of Foreign Experts Affairs of China 111 Project under Grant No. D16002.

## References


[1] Sales BC, Mandrus D, Williams RK. Filled skutterudite antimonides: A new class of thermoelectric materials. *Science* 1996, **272**: 1325–1328.

[2] Shi X, Kong H, Li C-P, *et al.* Low thermal conductivity and high thermoelectric figure of merit in n-type $Ba_xYb_yCo_4Sb_{12}$ double-filled skutterudites. *Appl Phys Lett* 2008, **92**: 182101.

[3] Leithe-Jasper A, Kaczorowski D, Rogl P, *et al.* Synthesis, crystal-structure determination and physical properties of $YbFe_4Sb_{12}$. *Solid State Commun* 1999, **109**: 395–400.

[4] Nolas GS, Kaeser M, Littleton RT, *et al.* High figure of merit in partially filled ytterbium skutterudite materials. *Appl Phys Lett* 2000, **77**: 1855–1857.

[5] Dilley NR, Bauer ED, Maple MB, *et al.* Thermoelectric properties of chemically substituted skutterudites $Yb_yCo_4Sn_xSb_{12-x}$. *J Appl Phys* 2000, **88**: 1948–1951.

[6] Park Y-S, Thompson T, Kim Y, *et al.* Protective enamel coating for n- and p-type skutterudite thermoelectric materials. *J Mater Sci* 2015, **50**: 1500–1512.

[7] Zhu T, Liu Y, Fu C, *et al.* Compromise and synergy in high-efficiency thermoelectric materials. *Adv Mater* 2017, **29**: 1605884

[8] Sales BC, Mandrus D, Chakoumakos BC, *et al.* Filled skutterudite antimonides: Electron crystals and phonon glasses. *Phys Rev B* 1997, **56**: 15081–15089.

[9] Mandrus D, Sales BC, Keppens V, *et al.* Filled skutterudite antimonides: Validation of the electron-crystal phonon-glass approach to new thermoelectric materials. *MRS Proceedings* 1997, **478**: 199.

[10] Sheet G, Rosner H, Wirth S, *et al.* High spin polarization in the ferromagnetic filled skutterudites $KFe_4Sb_{12}$ and $NaFe_4Sb_{12}$. *Phys Rev B* 2005, **72**: 180407.

[11] Pei YZ, Chen LD, Zhang W, *et al.* Synthesis and thermoelectric properties of $K_yCo_4Sb_{12}$. *Appl Phys Lett* 2006, **89**: 221107.

[12] Zhao XY, Shi X, Chen LD, *et al.* Synthesis and thermoelectric properties of Sr-filled skutterudite $Sr_yCo_4Sb_{12}$. *J Appl Phys* 2006, **99**: 053711.

[13] Chen LD, Kawahara T, Tang XF, *et al.* Anomalous barium filling fraction and n-type thermoelectric performance of $Ba_yCo_4Sb_{12}$. *J Appl Phys* 2001, **90**: 1864–1868.

[14] Kang Y, Yu F, Chen C, *et al.* High pressure synthesis and thermoelectric properties of Ba-filled $CoSb_3$ skutterudites. *J Mater Sci: Mater Electron* 2017, **28**: 8771–8776.

[15] Koza MM, Johnson MR, Viennois R, *et al.* Breakdown of phonon glass paradigm in La- and Ce-filled $Fe_4Sb_{12}$ skutterudites. *Nat Mater* 2008, **7**: 805–810.

[16] Feldman JL, Singh DJ, Kendziora C, *et al.* Lattice dynamics of filled skutterudites: $La(Fe, Co)_4Sb_{12}$. *Phys Rev B* 2003, **68**: 094301.

[17] Alboni PN, Ji X, He J, *et al.* Thermoelectric properties of $La_{0.9}CoFe_3Sb_{12}$–$CoSb_3$ skutterudite nanocomposites. *J Appl Phys* 2008, **103**: 113707.

[18] Tang XF, Chen LD, Goto T, *et al.* Synthesis and thermoelectric properties of filled skutterudite compounds $Ce_yFe_xCo_{4-x}Sb_{12}$ by solid state reaction. *J Mater Sci* 2001, **36**: 5435–5439.

[19] Pei YZ, Bai SQ, Zhao XY, *et al.* Thermoelectric properties of $Eu_yCo_4Sb_{12}$ filled skutterudites. *Solid State Sci* 2008, **10**: 1422–1428.

[20] Lamberton Jr. GA, Bhattacharya S, Littleton IV RT, *et al.* High figure of merit in Eu-filled $CoSb_3$-based skutterudites. *Appl Phys Lett* 2002, **80**: 598–600.

[21] Zhang Q, Chen C, Kang Y, *et al.* Structural and thermoelectric characterizations of samarium filled $CoSb_3$ skutterudites. *Mater Lett* 2015, **143**: 41–43.

[22] Artini C, Zanicchi G, Costa GA, *et al.* Correlations between structural and electronic properties in the filled skutterudite $Sm_y(Fe_xNi_{1-x})_4Sb_{12}$. *Inorg Chem* 2016, **55**: 2574–2583.

[23] Rogl G, Grytsiv A, Bauer E, *et al.* Thermoelectric properties of novel skutterudites with didymium: $DD_y(Fe_{1-x}Co_x)_4Sb_{12}$ and $DD_y(Fe_{1-x}Ni_x)_4Sb_{12}$. *Intermetallics* 2010, **18**: 57–64.

[24] Sayles TA, Baumbach RE, Yuhasz WM, *et al.* Superconductivity and crystalline electric field effects in the filled skutterudite $PrRu_4As_{12}$. *Phys Rev B* 2010, **82**: 104513.

[25] Shi X, Yang J, Chen LD, *et al.* Materials genome approach to accelerate thermoelectric material performance optimization. *Sci Technol Rev* 2015, **33**: 60–63.

[26] Shi X, Zhang W, Chen LD, *et al.* Filling fraction limit for intrinsic voids in crystals: Doping in skutterudites. *Phys Rev Lett* 2005, **95**: 185503.

[27] Zhao XY, Shi X, Chen LD, *et al.* Synthesis of $Yb_yCo_4Sb_{12}/Yb_2O_3$ composites and their thermoelectric properties. *Appl Phys Lett* 2006, **89**: 092121.

[28] Salvador JR, Yang J, Shi X, *et al.* Transport and mechanical properties of Yb-filled skutterudites. *Philos Mag* 2009, **89**: 1517–1534.

[29] Wang Y, Mao J, Jie Q, *et al.* Filling fraction of Yb in $CoSb_3$ skutterudite studied by electron microscopy. *Appl Phys Lett* 2017, **110**: 163901.

[30] Lee J-K, Choi S-M, Seo W-S, *et al.* Thermoelectric properties of spark plasma sintered $In_xYb_yLa_{0.3-x-y}Co_4Sb_{12}$ skutterudite system. *Renew Energ* 2012, **42**: 36–40.

[31] Dahal T, Jie Q, Joshi G, *et al.* Thermoelectric property enhancement in Yb-doped n-type skutterudites $Yb_xCo_4Sb_{12}$. *Acta Mater* 2014, **75**: 316–321.

[32] Ballikaya S, Uher C. Enhanced thermoelectric performance of optimized Ba, Yb filled and Fe substituted skutterudite compounds. *J Alloys Compd* 2014, **585**: 168–172.

[33] Son G, Lee KH, Choi S-M. Enhanced thermoelectric properties of melt-spun p-type $Yb_{0.9}Fe_3CoSb_{12}$. *J Electron Mater* 2017, **46**: 2839–2843.

[34] Nolas GS, Fowler G, Yang J. Assessing the role of filler atoms on the thermal conductivity of filled skutterudites. *J Appl Phys* 2006, **100**: 043705.

[35] Rowe DM. *Thermoelectrics Handbook: Macro to Nano*.

CRC Press, 2005.

[36] Artini C, Carlini R. Influence of composition and thermal treatments on microhardness of the filled skutterudite $Sm_y(Fe_xNi_{1-x})_4Sb_{12}$. *J Nanosci Nanotechno* 2017, **17**: 1634–1639.

[37] Yao Z, Li XY, Tang YS, *et al.* Genomic effects of the quenching process on the microstructure and thermoelectric properties of $Yb_{0.3}Co_4Sb_{12}$. *J Electron Mater* 2015, **44**: 1890–1895.

[38] Xing J, Gu H, Gloter A, *et al.* Bismuth nanoprecipitation at grain boundaries during microstructural evolution in (Sr, Ba)$TiO_3$ ceramics. *Acta Mater* 2007, **55**: 5323–5332.

[39] Gu H, Nagano T, Zhan G-D, *et al.* Dynamic evolution of grain-boundary films in liquid-phase-sintered ultrafine silicon carbide material. *J Am Ceram Soc* 2003, **86**: 1753–1760.

[40] Yao Z, Qiu P-F, Li X-Y, *et al.* Investigation on quick fabrication of n-type filled skutterudites. *J Inorg Mater* 2016, **31**: 1375–1382.

[41] Ding J, Gu H, Qiu P, *et al.* Creation of $Yb_2O_3$ nanoprecipitates through an oxidation process in bulk Yb-filled skutterudites. *J Electron Mater* 2013, **42**: 382–388.

[42] Zebarjadi M, Esfarjani K, Dresselhaus MS, *et al.* Perspectives on thermoelectrics: From fundamentals to device applications. *Energy Environ Sci* 2012, **5**: 5147–5162.